Going with the floe: tracking CESM Large Ensemble sea ice in the Arctic provides context for ship-based observations

Alice K. DuVivier[1], Patricia DeRepentigny[2,3], Marika M. Holland[1], Melinda Webster[4], Jennifer E. Kay[2,5], Don Perovich[6]

[1]National Center for Atmospheric Research, Boulder, CO, 80307, USA
[2]Department of Atmospheric and Oceanic Sciences, University of Colorado, Boulder, CO, USA
[3]Institute for Arctic and Alpine Research, University of Colorado, Boulder, CO, USA
[4]NASA Goddard Space Flight Center, Greenbelt, MD, USA
[5]Institute for Research in Environmental Sciences, University of Colorado, Boulder, CO, USA
[6]Thayer School of Engineering, Dartmouth College, Hanover, NH, USA

Correspondence to: Alice K. DuVivier (duvivier@ucar.edu)

Abstract. In recent decades, Arctic sea ice has shifted toward younger, thinner, seasonal ice regime. Studying and understanding this "New" Arctic will be the focus of a year-long ship campaign beginning in autumn 2019. Lagrangian tracking of sea ice floes in the Community Earth System Model Large Ensemble (CESM-LE) allow for understanding conditions that a floe will experience throughout the calendar year. These model tracks can assist with campaign planning, put into context a single year of observations, and provide guidance on how observations can help with model development. The modelled floe tracks show a Transpolar Drift trajectory is likely, providing guidance for coordinating satellite, airborne, and ground observations. However, there is a smaller possibility of high-risk tracks, including possible melt of the floe before the end of a calendar year. Because of high variability in the melt season sea ice conditions, we recommend *in-situ* sampling over a large range of ice conditions for a more complete understanding of how ice type or surface condition affect processes. We find that sea ice predictability emerges rapidly during the autumn freeze-up and anticipate that process-based observations during this period may help elucidate the processes leading to this change in predictability. Accurate seasonal cycle comparison of sea ice conditions between point-based observations a model requires the model to use a Lagrangian framework.

1 Introduction

In recent decades, sea ice in the Arctic Ocean has undergone rapid change (Serreze & Stroeve, 2015; Stroeve et al., 2011, 2012; Stroeve & Notz, 2018). Passive microwave satellite observations since 1979 show that Arctic sea ice extent has decreased in all months, and the twelve lowest September sea ice extents in the satellite record were recorded in the past twelve years (Richter-Menge pers. comm.). The reduced sea ice cover has local effects on boundary layer clouds,

temperature, and humidity, which can then feedback on the sea ice evolution (Boisvert & Stroeve, 2015; Kay & Gettelman, 2009; Morrison et al., 2018) and the large scale atmospheric circulation (e.g., Alexander, 2004; Barnes & Screen, 2015; Deser et al., 2016).

Year-round *in-situ* observations are critical for understanding the coupled air-sea-sea ice processes over the remote Arctic
35 Ocean, but they pose enormous challenges. The Surface Heat Budget of the Arctic (SHEBA) project obtained year-round, process-based observations over sea ice when the Canadian Coast Guard icebreaker Des Groseilliers was frozen into the Beaufort Sea and drifted freely with the pack from October 1997 to October 1998 (Uttal et al., 2002). SHEBA observations have been immensely helpful for process-based understanding of the coupled system, and have been widely used to improve modelling of processes in the polar regions (e.g., Bromwich et al., 2009; Intrieri et al., 2002; Klein et al., 2009). Since the
40 late 1990s when SHEBA occurred, there has been year-round sea ice loss (Stroeve & Notz, 2018), there is more first-year sea ice compared to multiyear ice (Maslanik et al., 2011; Nghiem et al., 2007), the pack has thinned substantially (Kwok, 2018; Kwok et al., 2009), and the melt season length has increased (Stammerjohn et al., 2012; Stroeve et al., 2016). Whether or not year-round coupled processes are similar in this new regime of young, thin, seasonal sea ice is an open question.

The international Multidisciplinary drifting Observatory for the Study of Arctic Climate (MOSAiC) experiment has been
45 designed to answer the question: what are the causes and consequences of an evolving and diminished Arctic sea ice cover? MOSAiC has been designed both to assess coupled air-sea-sea ice processes as well as to investigate the impact on ecosystems and biogeochemistry of the changing system. These observations are necessary to answer MOSAiC's driving question and improve our understanding and modelling of polar processes in a changing climate (Dethloff et al., 2016). In autumn 2019, the icebreaker RV Polarstern will be frozen into the Siberian Arctic with the aim of traversing the Transpolar
50 Drift over the following year. Because of differences in location and mean ice state, planning for MOSAiC based on experiences with SHEBA or satellite observations may not be illustrative of possible events. Additionally, awareness of the impact of internal climate variability on the possible range in sea ice conditions and the resulting representativeness of a single year of observations has been increasing over the recent years (Jahn et al., 2016; Swart et al., 2015).

In this study, we use a Lagrangian tracking system with data from 30 members of the publicly available Community Earth
55 System Model (CESM) Large Ensemble (CESM-LE) project (Kay et al., 2015) to derive sea ice tracks and state associated with each floe as it evolves over a calendar year. Three fundamental goals of this work are to: (1) assist with planning the campaign; (2) to provide guidance about what types of observations can best assist with model improvement; and (3) to offer insight on the representativeness of MOSAiC observations. In section 2, we describe the Lagrangian tracking and the CESM-LE and observational data used in this study. Subsequently, section 3 describes the resulting Lagrangian tracks, sea
60 ice conditions along the tracks, and initial value predictability. We conclude and discuss resulting recommendations for both sea ice observations and models in section 4.

2 Data and Methods

The CESM-LE is designed to assess the role of internal variability within the climate system. Comparisons between ensemble members allow us to better understand and contextualize the range of possible floe tracks, sea ice conditions, variability, and sea ice predictability. Each CESM-LE member uses an identical code base and external historical and future climate forcing, but has a round-off level atmospheric perturbation that leads to unique initialization in 1920. The CESM-LE well captures the Arctic sea ice historical state and trends (Barnhart et al., 2015; Jahn et al., 2016), the sea ice thickness (Labe et al., 2018), and the sea ice motion is reasonable though the CESM-LE Beaufort Gyre circulation is stronger than observed due to a bias in the simulated atmospheric circulation over the Arctic Ocean during the ice-covered season (DeRepentigny et al., 2016).

For this study, 30 CESM-LE members provide daily sea ice concentration and velocity (u and v) fields. We also use satellite-derived sea ice velocity (Tschudi et al., 2016) and concentration (Meier et al., 2017) from 1988-2016, for a total of 28 year-long observationally-derived drift tracks. We use the Lagrangian Ice Tracking System (LITS; DeRepentigny et al., 2016) to track virtual sea ice floes starting from the point 85°N, 125°E on October 15 (provided by MOSAiC campaign organizers) for: (1) satellite-derived historical conditions, (2) Perennial Arctic conditions, and (3) Seasonal Arctic conditions. We obtained simulated along-track floe characteristics (e.g. sea ice thickness, snow thickness, turbulent heat fluxes) for each of the unique tracks by using a weighted average of all model grid cells within 50 km of the latitude and longitude provided by LITS on that day.

For this paper, the term "Seasonal" ("Perennial") corresponds to drifts from October 15, 2021 (1980) to October 15, 2022 (1981). The fundamental distinction between these regimes is the transition from old, thick, perennial sea ice to young, thin, more seasonal sea ice (Perovich, 2011). The years of model data were chosen based on availability and clear representations of Perennial and Seasonal conditions. To evaluate the sensitivity of our results to the start location, we also ran LITS for a range of starting locations in the Siberian Arctic within +/- 5° latitude or longitude of 85°N, 125°E. While there were small changes in the floe track locations, the results were not significantly different from those presented here (not shown).

3 Results

3.1 Floe Tracks

To understand whether the shift from Perennial to Seasonal sea ice can lead to changes in likely floe paths, we use the LITS tracks to obtain statistical information relevant to planning an experiment's year-long drift. For the satellite-derived drifts, more recent years tend to have longer drift distances (not shown), indicating that thinner ice may lead to longer travel. While both the Seasonal and Perennial CESM-LE mean track distances are longer than the satellite-derived tracks indicating the

model ice speeds are faster than observations, the Seasonal tracks tend to travel further than Perennial tracks (Table 1). Therefore, it is likely that an experiment like MOSAiC drifting in thin ice conditions will travel further than it would have when the sea ice was thicker due to observed faster drift speeds for thinner ice (Morison & Goldberg, 2012; Rampal et al., 2009; Tschudi et al., 2019). Additionally, we find that five Seasonal tracks (17%) melt before October 15 of the following

95 year, with the earliest melt date on July 29 and the latest on September 22. Consequently, there is emerging risk that the floe may melt out before the end of a calendar year.

Examining individual tracks (Fig.1, grey lines) provides perspective about paths the icebreaker might travel within a year including high-risk paths. Figure 1 shows four different sectors in which the floe will end a year-long drift: a Russian Sector, a Canadian Sector, a Transpolar Drift sector, and a North Pole sector. Over the 1988-2015 period the satellite-derived tracks

100 most frequently end in the Transpolar Drift (46%; 13 tracks). In the first half of the observational record, prior to 2002, many tracks end near the North Pole sector (6 tracks) or enter the Russian sector (6 tracks). In later years, after 2002, the satellite-derived paths tend to shift toward the Canadian sector (not shown), though most ultimately end with a Transpolar Drift path (11 tracks). For the CESM-LE, the likely end points for tracks shift from the North Pole sector (63%) for Perennial to Transpolar Drift (47%) for Seasonal. Therefore, with thinner sea ice, both the observations and model show increased

105 frequency of Transpolar Drift tracks, which is important for planning logistics through the duration of the year-long experiment. Of additional concern is the possibility the track may enter a nation's exclusive economic zone (EEZ) because of potential impacts on campaign activities. In particular, if the experiment enters the Russian EEZ there may be an immediate cessation of all measurements, so understanding the likelihood of this occurrence in Seasonal sea ice conditions is important. Three satellite-derived tracks enter the Russian EEZ, while for CESM-LE only one Seasonal and Perennial track,

110 respectively, enters the Russian EEZ. Tests using different starting locations (not shown) suggest that starting locations within 5° further south or west (i.e. toward 0°E) results in more tracks that enter the Russian EEZ, underscoring the importance of the starting location. The CESM-LE tracks tend to have higher probability of ending in the Canadian region, which may be related to modelled centre of the Beaufort Gyre being displaced towards the Eurasian coastline, such that the resulting model tracks tend to be shifted toward the Canadian sector (DeRepentigny et al., 2016).

115 We created maps showing the number of times each grid cell is visited by sea ice tracks over two-week periods throughout the year (Fig. S1). These maps are also used to identify "likely" tracks by identifying locations with high track counts that also formed a continuous path (Fig.1, rainbow lines). While all likely tracks follow a Transpolar Drift, the likely Seasonal path is longer and shifted further towards the Canadian Arctic compared to the likely observed and Perennial paths, which end further north. These maps can also be used to inform the remote sensing community about the likelihood of when the

120 field experiment might be observable by satellites. Tracks in close proximity to the North Pole are not observable by satellites (approximately shown in Fig. 1 by the North Pole sector), and knowing when the floe is likely to be in these areas is valuable for planning and coordinating surface-based and airborne measurements to fill the high-latitude satellite "gap."

Equally, knowing where and when the track is likely to emerge from the satellite pole hole in spring after polar day has returned is valuable for planning visible image acquisition from satellites to support operational and scientific needs. All three "likely" tracks enter the satellite "gap" in December, but the difference in when the "likely" tracks exit the "gap" differs from the September period in observational and Perennial tracks but July in Seasonal tracks.

3.2 Seasonal Floe Conditions and Variability

The CESM-LE also provides guidance on likely sea ice conditions and variability that may be encountered during the year-long experiment and whether these have changed over time. Individual ensemble members provide unique realizations of equally-likely sea ice states, and the ensemble mean provides guidance on the most likely conditions.

The likely initial sea ice conditions are important both logistically and scientifically. Logistically, the likely initial ice state has implications on the icebreaker's ability to reach the desired destination and the fuel required. Scientifically, establishing an initial location that has a mix of multiyear and first year ice is important to ensure sampling of heterogeneous ice types. For Seasonal drifts, the starting location of 85°N, 125°E is likely to be within the sea ice pack (Fig. 2a), though it may be near the sea ice edge (e.g. Ens.2). The mean initial sea ice thickness is likely to be around 0.75 m (Fig. 2b), which is within the icebreaker's limitations. The mean ice age is around 1.75 years (Fig. 2c), indicating that there are likely to be multiyear floes in this location. The variability in the initial sea ice conditions is unsurprisingly higher for Seasonal than Perennial conditions, which were likely to have extensive, thick (>2 m), multiyear (>4 year) ice in this location (Fig. 3). The increase in variability indicates that finding the ideal mix of ice conditions for MOSAiC is less certain because of the large variability in individual ensemble members sea ice states at the campaign initiation.

The along-track sea ice state throughout the year for each unique Seasonal and Perennial track provides information about the seasonal evolution and variability in sea ice concentration and thickness. The sea ice concentration for all Seasonal and Perennial tracks is above 95% until about May 1, when the concentration begins to decrease (Fig. 4a, b). For Seasonal tracks, the initial ice thickness could range 0.2-2 m, though it is unlikely to exceed 3 m or fall below 1 m during the year-long drift (Fig. 4c). There is notable increase in melt season (taken here as May 1 to September 15) variability for Seasonal compared to Perennial. The average standard deviation for sea ice concentration is more than double for Seasonal (5.5%) compared to Perennial (2.6%) tracks. In contrast, the standard deviation in sea ice thickness is higher for Perennial (0.54 m) compared to Seasonal (0.38 m) floes because with thicker ice there was more multiyear ice that had the capability to be substantially thicker and therefore shift the variability (Fig.4d).

In addition to placing observations into context, we also address the challenge of evaluating modelled sea ice using single point observations. Compared to the Lagrangian along-track sea ice concentration, the polar-cap (70-90°N) average concentration and variability are lower, and the change in the rate of decline occurs earlier (Fig. 4a, b). This difference is

likely due to the along-track positions remaining at higher latitudes (>80° N) where they receive less sunlight and typically
melt later than sea ice would at lower latitudes (Bliss & Anderson, 2018). Because the timing of the seasonal cycles in pan-
155 Arctic, polar-cap averages is not an accurate representation of the seasonal cycle for a given floe, future model studies
comparing model output to MOSAiC observations should strive to use a Lagrangian comparison.

The variability as measured by standard deviation is also higher for Seasonal surface conditions that impact sea ice evolution
–snow fraction, pond fraction, and albedo (Fig. 5). Unsurprisingly, in a warmer climate like that associated with Seasonal
conditions, there tends to be higher pond fraction and lower snow cover fraction. Additionally, the standard deviation for
160 snow depth is higher for Perennial (0.15 m) compared to Seasonal (0.38 m) tracks because most Seasonal tracks experience
complete snow melt in July (Fig. 5d). In contrast, modelled Perennial tracks tend not to lose all their snow, which has been
previously documented in CESM simulations (Light et al., 2015). The snow differences impact the ice concentration
variability through the positive albedo feedback (Goosse et al., 2018; Hall, 2004; Qu & Hall, 2007), and as a result of these
surface conditions the Perennial tracks maintain a higher albedo throughout summer (Fig. 5a).

165 As a result of the difference in surface conditions, during the melt season the biggest difference in the Seasonal and
Perennial surface energy budget is from net shortwave radiation (Fig. 6a). The variability in the Seasonal energy budget
terms is much larger than the Perennial conditions (Fig. 6b, c). During the melt season, compared to Perennial tracks the
Seasonal tracks have more top melt initially but later differences in bottom melt become dominant (Fig. 6d), and the
variability is larger in the Seasonal conditions compared to Perennial conditions (Fig. 6e, f). For Seasonal tracks the loss of
170 snow increases surface shortwave absorption for both sea ice and the surrounding ocean, which leads to increases in top and
bottom melt (Perovich et al., 2007). The thickness variability may be damped in Seasonal tracks because of the negative ice
thickness-ice growth rate feedback (Bitz & Roe, 2004; Goosse et al., 2018), as thinner ice grows faster due to higher heat
conduction.

These results of conditions and energy and mass budgets along the floe tracks are particularly useful for a two-way exchange
175 of information: (1) they place context on a single year's worth of observations during a year-long field campaign, (2)
remotely-sensed observations along the modelled drift tracks from the year before, during, and after the MOSAiC campaign
can be collected to assess the magnitude of inter-annual variability of the modelled variables, and (3) the observations will
help constrain the range in variability shown by the model for sea ice and surface conditions.

3.3 Floe Predictability

180 The CESM-LE also provides the opportunity to explore the initial value predictability for the state of the expedition's sea ice
floe. For campaign planning purposes, it is important when establishing an initial ice camp to be confident that the sea ice
floes will be sufficiently stable to prevent endangering personnel or equipment. By calculating the autocorrelation coefficient

between the 30 unique initial floe conditions and the subsequent conditions each following month throughout the year, we are able to explore how long there is predictability in the sea ice system based on the initial sea ice state. In the CESM, the sea ice model represents subgrid-scale heterogeneity for five thickness categories (Hunke & Lipscomb, 2008), allowing us to consider the predictability of concentration by thickness category.

For Seasonal tracks with a campaign start date of October 15 there is high and significant correlation for grid-cell mean sea ice thickness between the initial value and values into June of the following year (Fig. 7a). While the autocorrelation is low for grid-cell mean sea ice concentration, the autocorrelation for concentration of ice in thicker categories is high which reflects the high initial value predictability of Arctic sea ice thickness (Blanchard-Wrigglesworth et al., 2011a, 2011b). The autocorrelation of all sea ice variables for a Seasonal floe is lower compared to Perennial autocorrelations initialized on October 15 (Fig. 7b), suggesting lower predictability. We tested other predictors (e.g. initial fraction of open water or sea surface temperature) for the sea ice floe's state at later dates during the campaign, but these were found to have low, statistically insignificant correlations immediately and therefore were poor predictors (not shown).

The exact start date of the campaign is indefinable, but may occur as early as October 1 or possibly as late as October 31. To understand how the predictability may change based on start date, we also evaluate the predictability characteristics for tracks initialized at the same location but on different dates. For Seasonal floes, an October 1 start date results in lower autocorrelations (Fig. 7c), while an October 30 start date has nearly identical autocorrelations (not shown) compared to an October 15 start date. In contrast, for a Perennial floe the autocorrelations are similar between October 1 and October 15 start date (Fig. 7d). Because sea ice state predictors change rapidly during these two weeks, predictors used in Perennial conditions during October may not be appropriate in Seasonal conditions at the same calendar date depending at the stage of freeze-up. The evolution of differences in predictability characteristics that emerge during the autumn freeze-up are not yet well understood.

4 Discussion and Conclusions

Tracking modelled sea ice floes using coupled CESM-LE climate model data provides a useful framework both for informing the planning of a large observational campaign like MOSAiC and also for putting into context a single year's observations. As the Polarstern searches for an initial floe from which to establish camp, at 85°N, 125°E there is likely to be widespread ice cover with a mix of predominantly new, thin ice and some old, thick ice. Starting from this location, a Transpolar Drift path is most likely (47%) in Seasonal conditions. From this initial location the floe may have a track shifted further toward the Beaufort Gyre than would be likely in Perennial conditions with thicker ice. However, tests with initial locations further south or west have higher risk of entering the Russian EEZ, which indicates the importance of the campaign's initial location. There is a small (17%) chance the floe may melt out in August or September before a full calendar year. These simulated paths can also be used to coordinate airborne or surface measurements with acquisition of

visible satellite imagery. We find that in a Seasonal Arctic, the campaign will likely be visible by satellites by July, which is
215   earlier than estimated using satellite observations or Perennial conditions. Ultimately, the path that MOSAiC takes can be
used to validate and improve modelled sea ice motion (e.g. Beaufort Gyre strength and location).

We also find that the best practice when comparing modelled data to observational point-based data that moves location is to
use a Lagrangian framework to analyse the model output rather than a regional average (e.g. Polar-Cap 70-90°N or Pan-
Arctic). There was a large discrepancy in the seasonal cycle for the average versus along a Lagrangian track because the
220   timing of the seasonal cycle for a particular floe near the pole is not well represented by a polar-cap average, primarily due to
differences in solar radiation for high latitude floes.

For the Seasonal Arctic, there is a large range in possible initial sea ice conditions, so the campaign may start at the ice edge
or within the pack. The variability in melt-season conditions is higher in the Seasonal than Perennial Arctic, so there is large
uncertainty in the initial sea ice state from which the campaign will start due to the large variability. A high-precision record
225   in one location for one sea ice type is just one realization in the wide range of possible sea ice states, so observations
spanning a diverse range of sea ice conditions are crucial for improving modelled processes of the heterogeneous sea ice
system. The initial MOSAiC camp will be established on a thick floe, which is likely to persist throughout the following
year, though large variability in melt season sea ice conditions should be expected. We recommend both *in-situ* sampling of
a large range in conditions as well as targeting airborne and spaceborne platforms on the anticipated drift tracks in the year
230   before, during, and after the MOSAiC campaign to better understand the variability within the system. Because sea ice
models represent subgrid-scale ice thickness categories and combines these into a coarser grid cell representation, it is
particularly valuable to obtain observations spanning a range of ice conditions in order to enable process-oriented
understanding and model representation over a fully-representative distribution of sea ice conditions.

While a thick initial sea ice floe for the campaign is likely to persist well into the following year, the emergence of
235   predictability during the autumn freeze-up is not well understood and was unexpected. Observations of processes occurring
during the autumn freeze-up will be beneficial for understanding the formation and evolution of the sea ice thickness
distribution and how this, in turn, affects sea ice predictability throughout the year.

Acknowledgements

This material is based upon work supported by the National Center for Atmospheric Research, which is a major facility
240   sponsored by the National Science Foundation (NSF) under Cooperative Agreement No. 1852977. The CESM project is
supported primarily by NSF, and computing and data storage resources, including the Cheyenne supercomputer
(doi:10.5065/D6RX99HX), were provided by the Computational and Information Systems Laboratory (CISL) at NCAR. P.
DeRepentigny acknowledges the support of the Natural Sciences and Engineering Council of Canada (NSERC), the Fond de

recherche Nature et Technologies du Québec (FRQNT) and the Canadian Meteorological and Oceanographic Society

245 (CMOS) through PhD scholarships. M. Holland acknowledges support from NSF (OPP 1724748); D. Perovich acknowledges support by NSF; J. Kay acknowledges support from NSF (CAREER 1554659). M. Webster is supported by the National Aeronautics and Space Administration's New Investigator Program in Earth Science. CESM-LE data are freely available: http://www.cesm.ucar.edu/projects/community-projects/LENS/. The scripts used for this analysis in this paper can be found here: https://github.com/duvivier/MOSAIC_TC_2019.

250 **References**

Alexander, M. A.: The Atmospheric Response to Realistic Arctic Sea Ice Anomalies in an AGCM during Winter. J. Clim., 17, 16, *https://doi.org/10.1175/1520-0442(2004)017<0890:TARTRA>2.0.CO;2*, 2004.

Barnes, E. A., & Screen, J. A.: The impact of Arctic warming on the midlatitude jet-stream: Can it? Has it? Will it?: Impact of Arctic warming on the midlatitude jet-stream, WIRES: Clim. Change, 6, 277–286, https://doi.org/10.1002/wcc.337, 2015.

255 Barnhart, K. R., Miller, C. R., Overeem, I., & Kay, J. E.: Mapping the future expansion of Arctic open water, Nature Climate Change, 6(3), 280–285, https://doi.org/10.1038/nclimate2848, 2015.

Bitz, C. M., & Roe, G. H.: A Mechanism for the High Rate of Sea Ice Thinning in the Arctic Ocean, J. Clim., 17, 10, *https://doi.org/10.1175/1520-0442(2004)017<3623:AMFTHR>2.0.CO;2*, 2004.

Blanchard-Wrigglesworth, E., Bitz, C. M., & Holland, M. M.: Influence of initial conditions and climate forcing on

260 predicting Arctic sea ice, Geophys. Res. Lett., 38(18), L18503, https://doi.org/10.1029/2011GL048807, 2011a.

Blanchard-Wrigglesworth, Edward, Armour, K. C., Bitz, C. M., & DeWeaver, E.: Persistence and Inherent Predictability of Arctic Sea Ice in a GCM Ensemble and Observations, J. Clim, 24(1), 231–250, https://doi.org/10.1175/2010JCLI3775.1, 2011b.

Boisvert, L. N., & Stroeve, J. C.: The Arctic is becoming warmer and wetter as revealed by the Atmospheric Infrared

265 Sounder, Geophys. Res. Lett., 42(11), 4439–4446, https://doi.org/10.1002/2015GL063775, 2015.

Bromwich, D. H., Hines, K. M., & Bai, L.-S.: Development and testing of Polar Weather Research and Forecasting model: 2. Arctic Ocean, J. Geophys. Res., 114(D8), D08122, https://doi.org/10.1029/2008JD010300, 2009.

DeRepentigny, P., Tremblay, L. B., Newton, R., & Pfirman, S.: Patterns of Sea Ice Retreat in the Transition to a Seasonally Ice-Free Arctic, J. Clim, 29(19), 6993–7008, https://doi.org/10.1175/JCLI-D-15-0733.1, 2016.

270   Deser, C., Sun, L., Tomas, R. A., & Screen, J.: Does ocean coupling matter for the northern extratropical response to projected Arctic sea ice loss?, Geophys. Res. Lett., 43(5), 2149–2157, https://doi.org/10.1002/2016GL067792, 2016.

Dethloff, K., Rex, M., & Shupe, M.: Multidisciplinary drifting Observatory for the Study of Arctic Climate (MOSAiC), Geophysical Research Abstracts, 18(EGU2016-3064), 1, 2016.

Goosse, H., Kay, J. E., Armour, K. C., Bodas-Salcedo, A., Chepfer, H., Docquier, D., et al.: Quantifying climate feedbacks
275   in polar regions, Nat. Comm., 9(1), 1919, https://doi.org/10.1038/s41467-018-04173-0, 2018.

Hall, A.: The Role of Surface Albedo Feedback in Climate, J. Clim., 17, 19, *https://doi.org/10.1175/1520-0442(2004)017<1550:TROSAF>2.0.CO;2*, 2004.

Hunke, E. C., & Lipscomb, W. H.: CICE: the Los Alamos Sea Ice Model Documentation and Software Version 4.0. Los Alamos National Laboratory, Los Alamos NM, LA-CC-06-012, 76, 2008.

280   Intrieri, J. M., Fairall, C. W., Shupe, M. D., Persson, P. O. G., Andreas, E. L., Guest, P. S., & Moritz, R. E.: An annual cycle of Arctic surface cloud forcing at SHEBA, J. Geophys. Res., 107(C10). https://doi.org/10.1029/2000JC000439, 2002.

Jahn, A., Kay, J. E., Holland, M. M., & Hall, D. M.: How predictable is the timing of a summer ice-free Arctic?, Geophys. Res. Lett., 43(17), 9113–9120, https://doi.org/10.1002/2016GL070067, 2016.

Kay, J. E., Deser, C., Phillips, A., Mai, A., Hannay, C., Strand, G., et al.: The Community Earth System Model (CESM)
285   Large Ensemble Project: A Community Resource for Studying Climate Change in the Presence of Internal Climate Variability, Bull. Amer. Meteorol. Soc., 96(8), 1333–1349, https://doi.org/10.1175/BAMS-D-13-00255.1, 2015.

Kay, Jennifer E., & Gettelman, A.: Cloud influence on and response to seasonal Arctic sea ice loss, J. Geophys. Res., 114(D18), https://doi.org/10.1029/2009JD011773, 2009.

Klein, S. A., McCoy, R. B., Morrison, H., Ackerman, A. S., Avramov, A., Boer, G. de, et al.: Intercomparison of model
290   simulations of mixed-phase clouds observed during the ARM Mixed-Phase Arctic Cloud Experiment. I: single-layer cloud, Q. J. Royal Meteorol. Soc., 135(641), 979–1002, https://doi.org/10.1002/qj.416, 2009.

Kwok, R: Arctic sea ice thickness, volume, and multiyear ice coverage: losses and coupled variability (1958–2018), Env. Res. Lett., 13(10), 105005, https://doi.org/10.1088/1748-9326/aae3ec, 2018.

Kwok, R., Cunningham, G. F., Wensnahan, M., Rigor, I., Zwally, H. J., & Yi, D.: Thinning and volume loss of the Arctic
295   Ocean sea ice cover: 2003–2008, J. Geophys. Res. Oceans, 114(C7), C07005, https://doi.org/10.1029/2009JC005312, 2009.

Labe, Z., Magnusdottir, G., & Stern, H.: Variability of Arctic Sea Ice Thickness Using PIOMAS and the CESM Large Ensemble, J. Clim, 31(8), 3233–3247, https://doi.org/10.1175/JCLI-D-17-0436.1, 2018.

Lamarque, J.-F., Kyle, G. P., Meinshausen, M., Riahi, K., Smith, S. J., van Vuuren, D. P., et al.: Global and regional evolution of short-lived radiatively-active gases and aerosols in the Representative Concentration Pathways, Clim. Change, 300   109(1–2), 191–212. https://doi.org/10.1007/s10584-011-0155-0, 2011.

Maslanik, J., Stroeve, J., Fowler, C., & Emery, W.: Distribution and trends in Arctic sea ice age through spring 2011: Geophys. Res. Lett., 38(13), https://doi.org/10.1029/2011GL047735, 2011.

Meier, W. N., Fetterer, F., Savoie, M. H., Mallory, S., Duerr, R., & Stroeve, Julienne C.: NOAA/NSIDC Climate Data Record of Passive Microwave Sea Ice Concentration, Version 3. [1988-2016]. Retrieved November 30, 2018, from 305   https://doi.org/10.7265/N59P2ZTG, 2017

Meinshausen, M., Smith, S. J., Calvin, K., Daniel, J. S., Kainuma, M. L. T., Lamarque, J.-F., et al.: The RCP greenhouse gas concentrations and their extensions from 1765 to 2300, Clim. Change, 109(1–2), 213–241, https://doi.org/10.1007/s10584-011-0156-z, 2011.

Morrison, A. L., Kay, J. E., Frey, W. R., Chepfer, H., & Guzman, R.: Cloud Response to Arctic Sea Ice Loss and 310   Implications for Future Feedbacks in the CESM1 Climate Model, J. Geophys. Res. Atmos., https://doi.org/10.1029/2018JD029142, 2018.

Nghiem, S. V., Rigor, I. G., Perovich, D. K., Clemente-Colón, P., Weatherly, J. W., & Neumann, G.: Rapid reduction of Arctic perennial sea ice, Geophys. Res. Lett., 34(19), L19504, https://doi.org/10.1029/2007GL031138, 2007.

Perovich, D.:The Changing Arctic Sea Ice Cover. Oceanography, 24(3), 162–173, https://doi.org/10.5670/oceanog.2011.68, 315   2011.

Perovich, D. K., Light, B., Eicken, H., Jones, K. F., Runciman, K., & Nghiem, S. V.: Increasing solar heating of the Arctic Ocean and adjacent seas, 1979–2005: Attribution and role in the ice-albedo feedback, Geophys. Res. Lett., 34(19), L19505, https://doi.org/10.1029/2007GL031480, 2007.

Qu, X., & Hall, A.: What Controls the Strength of Snow-Albedo Feedback?, J. Clim., 20(15), 3971–3981, 320   https://doi.org/10.1175/JCLI4186.1, 2007.

Richter-Menge, personal communication. (Prepared for) The Arctic [in "State of the Climate in 2018"]. Bulletin of the American Meteorological Society, 2018.

Serreze, M. C., & Stroeve, J.: Arctic sea ice trends, variability and implications for seasonal ice forecasting, Philos. Trans. Royal Soc. A, 373(2045), 20140159. https://doi.org/10.1098/rsta.2014.0159, 2015.

325 Stammerjohn, S., Massom, R., Rind, D., & Martinson, D.: Regions of rapid sea ice change: An inter-hemispheric seasonal comparison, Geophys. Res. Lett., 39(6), https://doi.org/10.1029/2012GL050874, 2012.

Stroeve, J., & Notz, D.: Changing state of Arctic sea ice across all seasons, Env. Res. Lett., 13(10), 103001, https://doi.org/10.1088/1748-9326/aade56, 2018.

Stroeve, J. C., Serreze, M. C., Holland, M. M., Kay, J. E., Malanik, J., & Barrett, A. P.: The Arctic's rapidly shrinking sea
330 ice cover: a research synthesis, Climatic Change, 110, 1005–1027, https://doi.org/10.1007/s10584-011-0101-1, 2011.

Stroeve, J. C., Kattsov, V., Barrett, A., Serreze, M., Pavlova, T., Holland, M., & Meier, W. N.: Trends in Arctic sea ice extent from CMIP5, CMIP3 and observations, Geophys. Res. Lett., 39(16), L16502, https://doi.org/10.1029/2012GL052676, 2012.

Stroeve, J. C., Crawford, A. D., & Stammerjohn, S., Using timing of ice retreat to predict timing of fall freeze-up in the
335 Arctic, Geophys. Res. Lett., 43(12), 6332–6340, https://doi.org/10.1002/2016GL069314, 2016.

Swart, N. C., Fyfe, J. C., Hawkins, E., Kay, J. E., & Jahn, A.: Influence of internal variability on Arctic sea-ice trends, Nat. Clim. Change, 5(2), 86–89, https://doi.org/10.1038/nclimate2483, 2015.

Tschudi, M. A., Fowler, C., Maslanik, J. A., Stewart, J. S., & Meier, W. N. (2016, to present). Polar Pathfinder Daily 25 km EASE-Grid Sea Ice Motion Vectors, Version 3. [1988-2016]. Retrieved March 20, 2019, from
340 https://doi.org/10.5067/O57VAIT2AYYY

Uttal, T., Curry, J. A., Mcphee, M. G., Perovich, D. K., Moritz, R. E., Maslanik, J. A., et al.: Surface Heat Budget of the Arctic Ocean, Bull. Amer. Meteor. Soc., 83(2), 255–275, https://doi.org/10.1175/1520-0477(2002)083<0255:SHBOTA>2.3.CO;2, 2002.

345

	Satellite	Seasonal CESM-LE	Perennial CESM-LE
Total # tracks	28 tracks	30 tracks	30 tracks
Average Distance	2018 km	2944 km	2572 km
Standard Deviation	416 km	196 km	173 km
Maximum Distance	2719 km	3379 km	2915 km
Minimum Distance	1339 km	2594 km	2104 km
Melts before calendar year	0 tracks	5 tracks	0 tracks
North Pole endpoint	8 tracks	10 tracks	19 tracks
Transpolar Drift endpoint	13 tracks	14 tracks	8 tracks
Russian endpoint	7 tracks	1 track	1 track
Canadian endpoint	0 tracks	5 tracks	2 tracks

Table 1: Statistics for LITS model tracks for satellite observations and Seasonal and Perennial CESM-LE. The different endpoint regions (illustrated on Figure 1) are defined with final latitude/longitude values as follows: North Pole (Lat. ≥ 87°); Transpolar drift (Lat. < 87°, 35° > Lon. > -60°); Russian (Lat. < 87°, 180° ≥ Lon. ≥ 35°); Canadian (Lat. < 87°, 60° ≥ Lon. ≥ -180°).
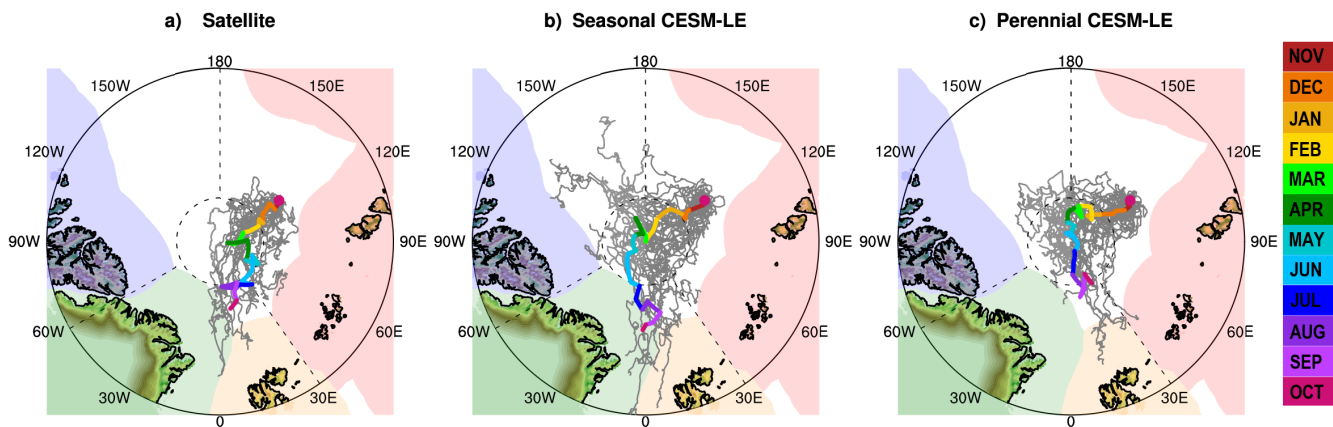
Figure 1: Unique ice floe tracks (grey) for satellite observations (a), Seasonal (b) and Perennial (c) CESM-LE ensembles. Likely tracks (rainbow with corresponding months shown at far right) based on the individual tracks are overlain. Dashed lines indicate boundaries for Transpolar Drift, North Pole, Russian, and Canadian regions described in Table 1. National exclusive economic zones (EEZ) for Russia (red), Norway (gold), Greenland (green), and Canada (blue) are shaded.
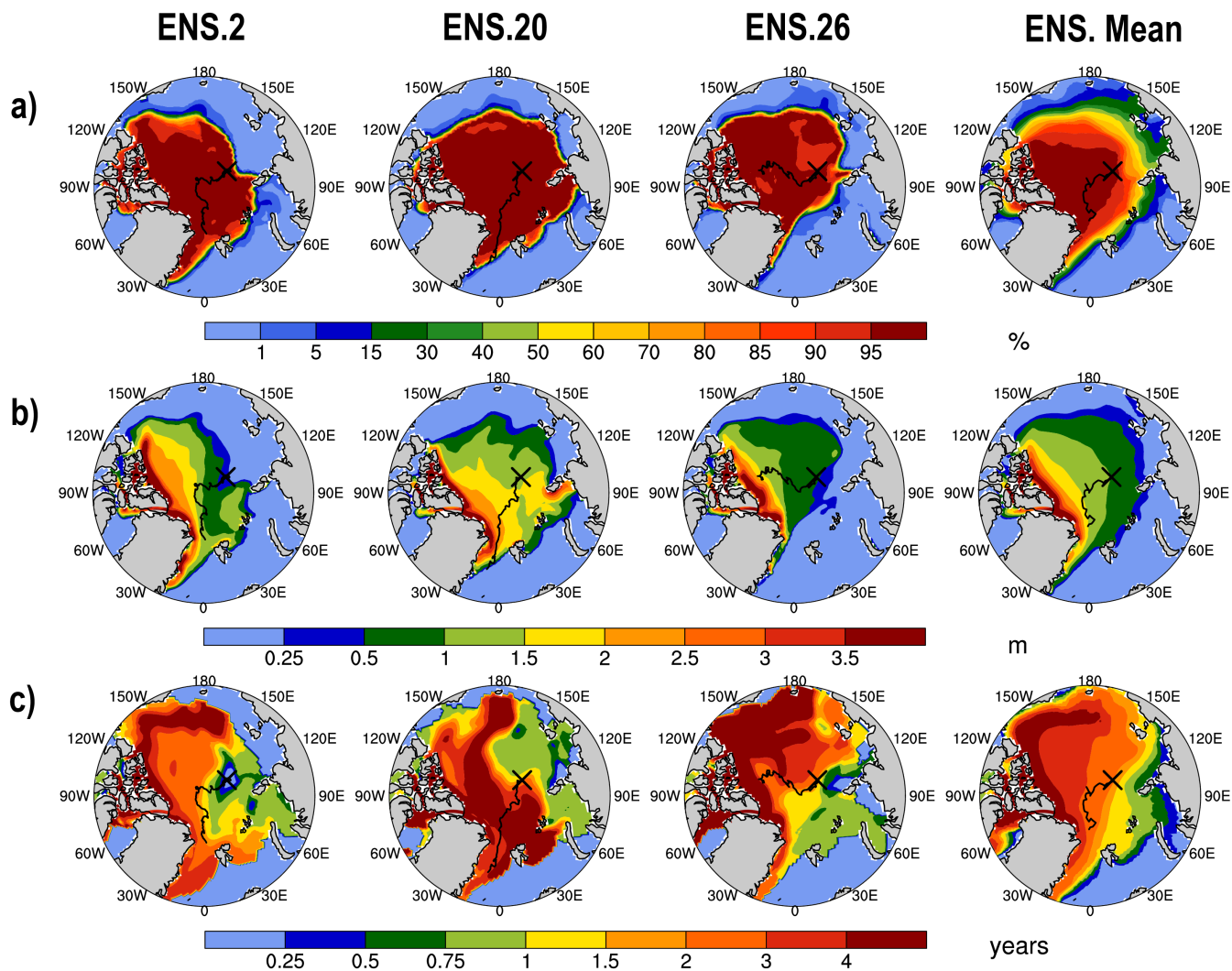
355

Figure 2: Seasonal grid cell daily mean sea ice concentration (a), thickness (b), and ice age (c) on Oct.15. Three random ensembles from the CESM-LE and ensemble mean are shown. The black 'X' in each map denotes the campaign starting location. Overlain as black lines are the Lagrangian track for each ensemble member and the highly probable track from Fig.1 for the Ensemble mean.
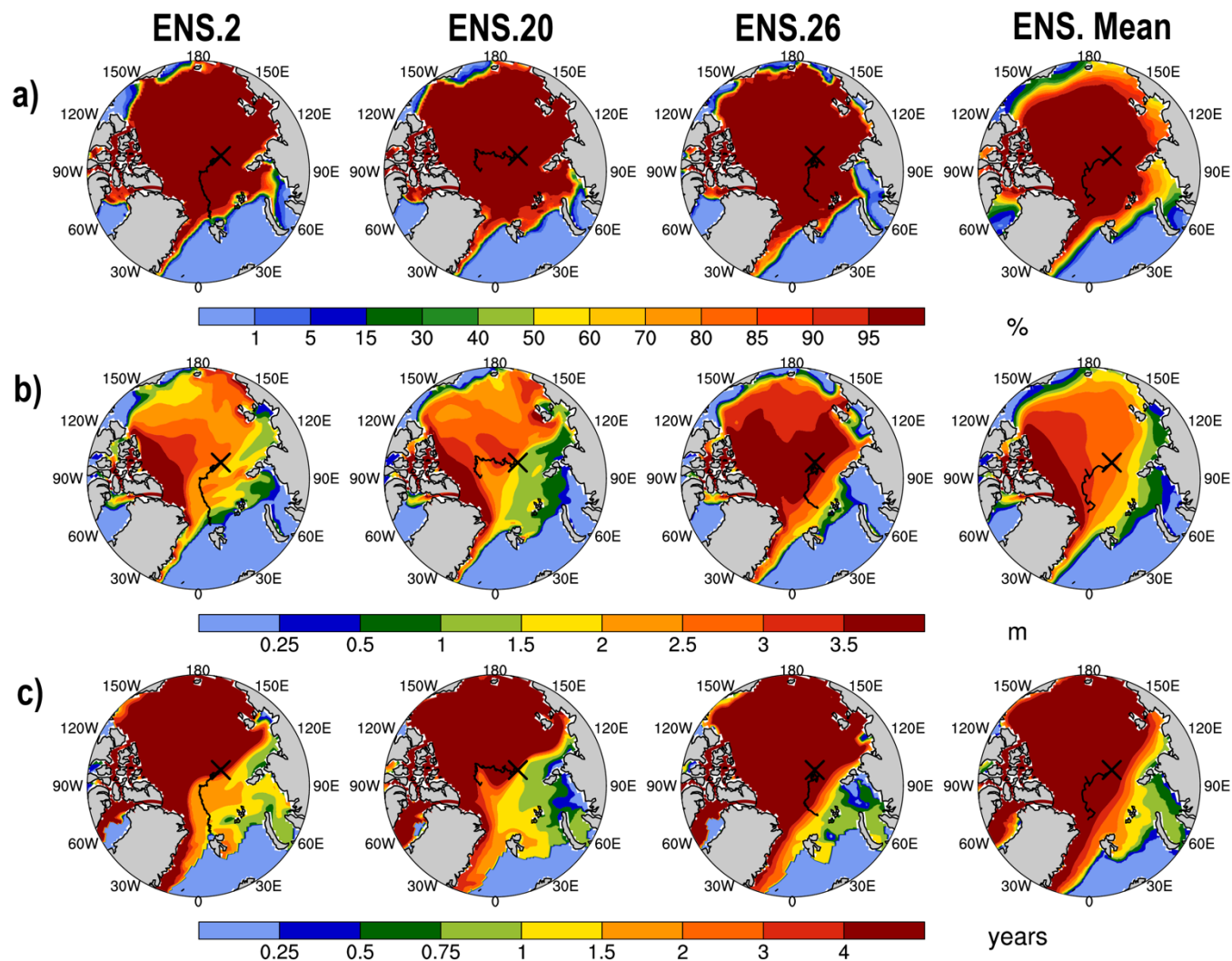
Figure 3: Perennial grid cell daily mean sea ice concentration (a), thickness (b), and ice age (c) on Oct.15. Three random ensembles from the CESM-LE and ensemble mean are shown. The black 'X' in each map denotes the campaign starting location. Overlain as black lines are the Lagrangian track for each ensemble member and the highly probable track from Fig.1 for the Ensemble mean.
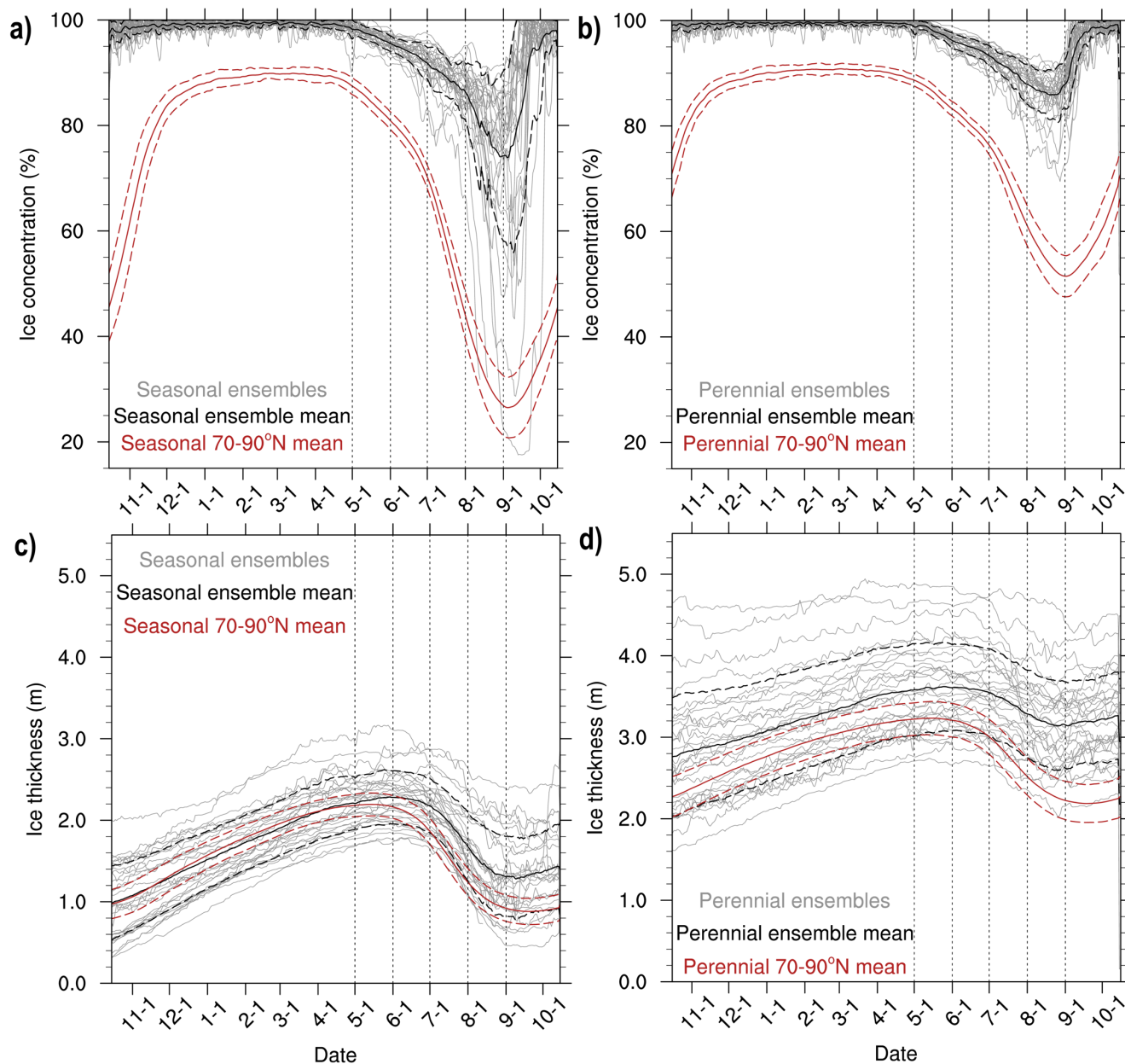
Figure 4: Perennial grid cell daily mean sea ice concentration (a), thickness (b), and ice age (c) on Oct.15. Three random ensembles from
365   the CESM-LE and ensemble mean are shown. The black 'X' in each map denotes the campaign starting location. Overlain as black lines
are the Lagrangian track for each ensemble member and the highly probable track from Fig.1 for the Ensemble mean.
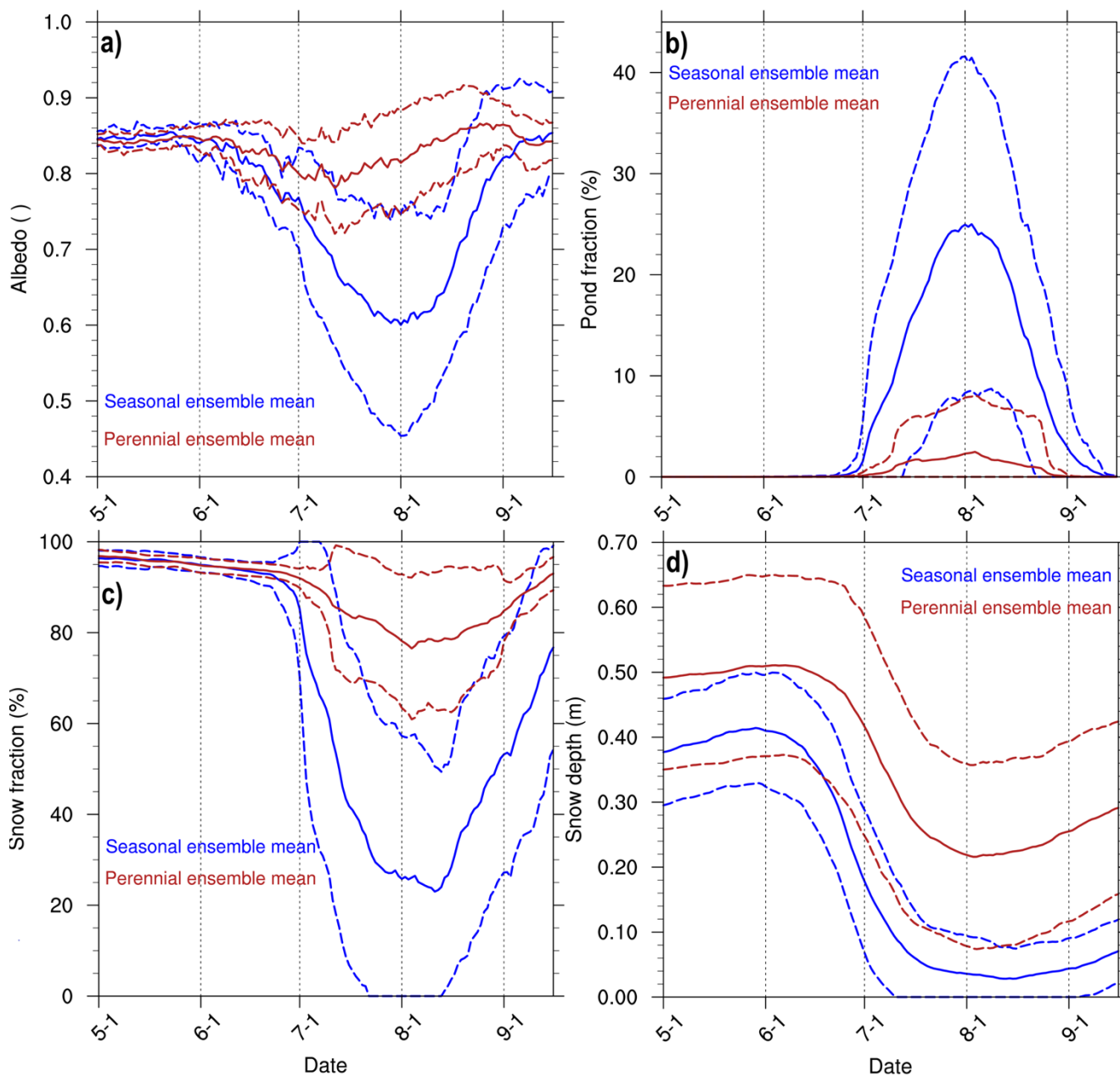
Figure 5: Melt season daily mean sea ice albedo (a), pond fraction of model grid cell (b), snow depth on sea ice (c), snow fraction on sea ice (d). The ensemble mean (solid) and +/-1 standard deviation envelope (dashed) are shown for Seasonal (blue) and Perennial (red) Arctic.
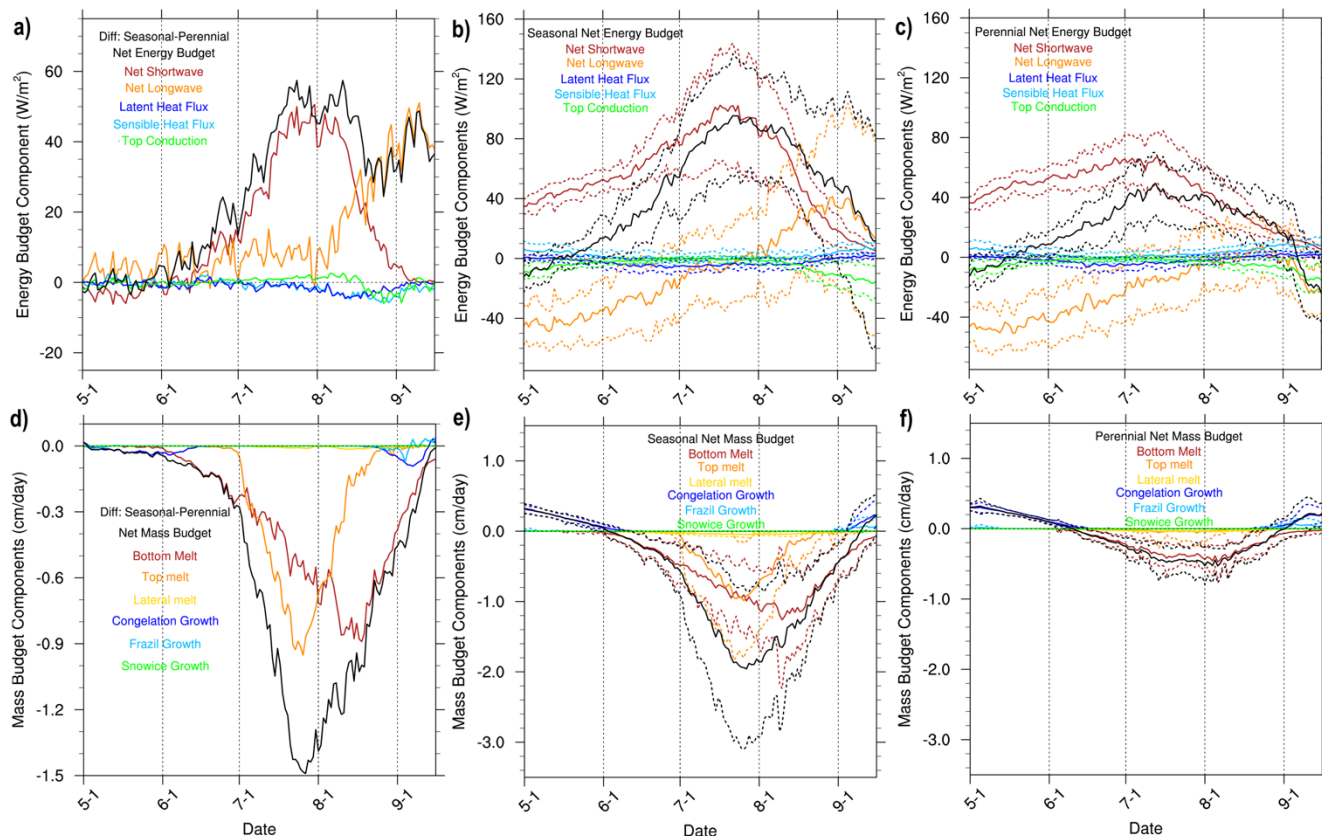
Figure 6: Melt season daily mean surface: energy budget differences (a) and components (b, c) and mass budget differences (d) and components (e, f). Differences are Seasonal tracks minus Perennial tracks. The ensemble mean (solid) and +/-1 standard deviation envelope (dashed) are shown. Components of the energy budget include: net (black), net shortwave (red), net longwave (orange), latent heat flux (dark blue), sensible heat flux (light blue), and top conductive flux (green). Components of the mass budget include: net (black), bottom melt (red), top melt (orange), lateral melt (gold), congelation growth (dark blue), frazil growth (light blue), and snow-ice growth (green).
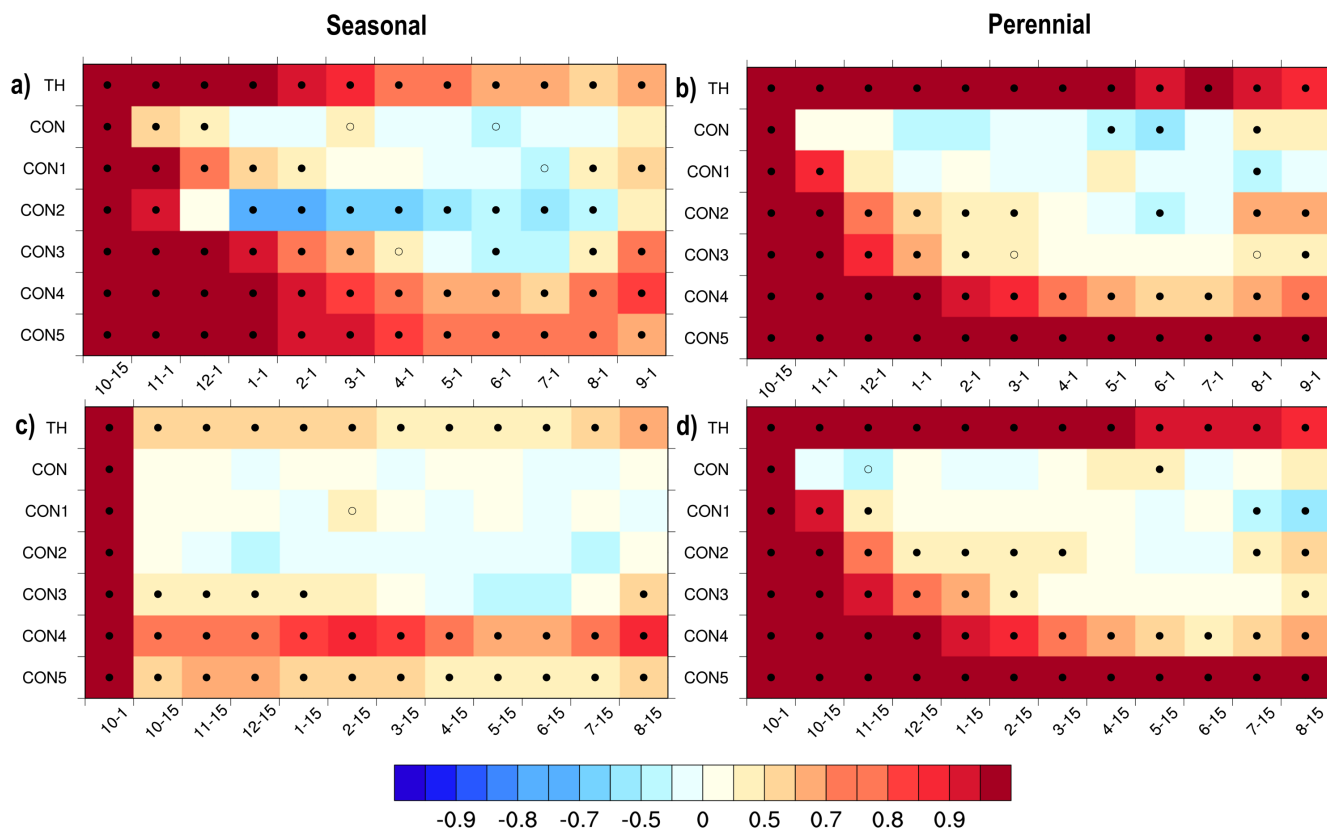
Figure 7: Correlation coefficients for sea ice variables between the initial condition and condition throughout the year for Seasonal (a, c) and Perennial (b, d) tracks initialized on Oct.15 (a, b; top row) and Oct.1 (c, d; bottom row). Solid (open) black dots indicate statistical significance at the 95% (90%) confidence level. From top to bottom, the variables shown are grid cell mean ice thickness (TH), grid cell mean ice concentration (CON), ice concentration for categories 1-5 (CON1-CON5) that correspond to the following thickness ranges: 0-0.59, 0.6-1.39, 1.4-2.39, 2.4-3.59, 3.6+ meters (Hunke & Lipscomb, 2008).